

Supplementary Information

Sequentially surface modified hematite enables lower applied bias photoelectrochemical water splitting

Andebet Gedamu Tamirat^a, Amare Aregahegn Dubale^a, Wei-Nien Su^{b*}, Hung-Ming Chen^a, and Bing-Joe Hwang^{*ac}

^aNanoElectrochemistry Laboratory, Department of Chemical Engineering, National Taiwan University of Science and Technology, Taipei, 106, Taiwan. E-mail: bjh@mail.ntust.edu.tw; Fax: +886-2-27376644

^bNanoElectrochemistry Laboratory, Graduate Institute of Applied Science and Technology, National Taiwan University of Science and Technology, Taipei 106, Taiwan

^cNational Synchrotron Radiation Research Center, Hsinchu, 30076, Taiwan

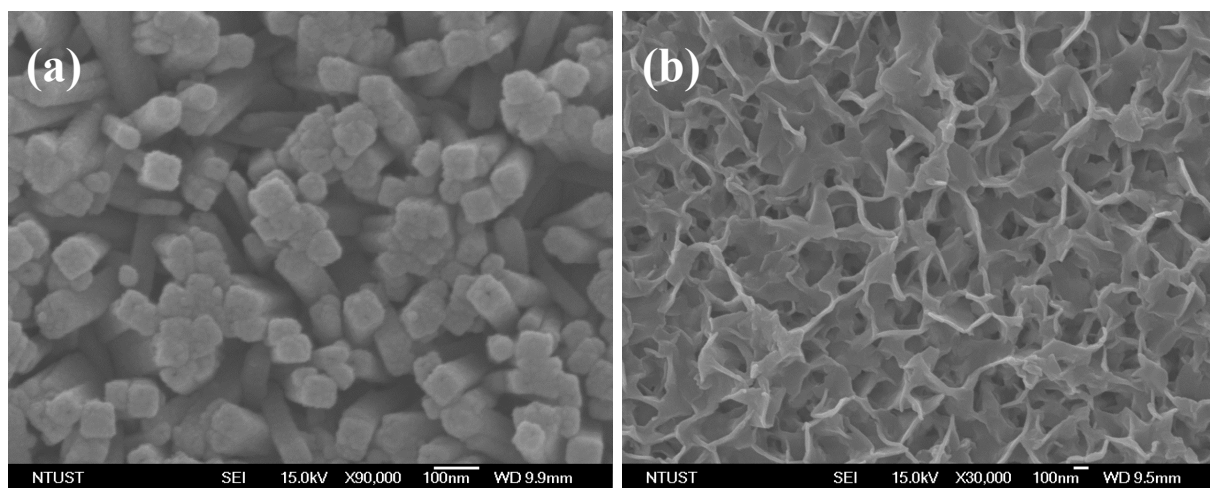


Figure S1. (a) As-prepared FeOOH sample treated with 4 cycles of Sn⁴⁺ solution before annealing. (b) SEM image of Fe₂O₃/Fe_{2-x}Sn_xO₃/NiOOH after 2 hr NiOOH deposition.

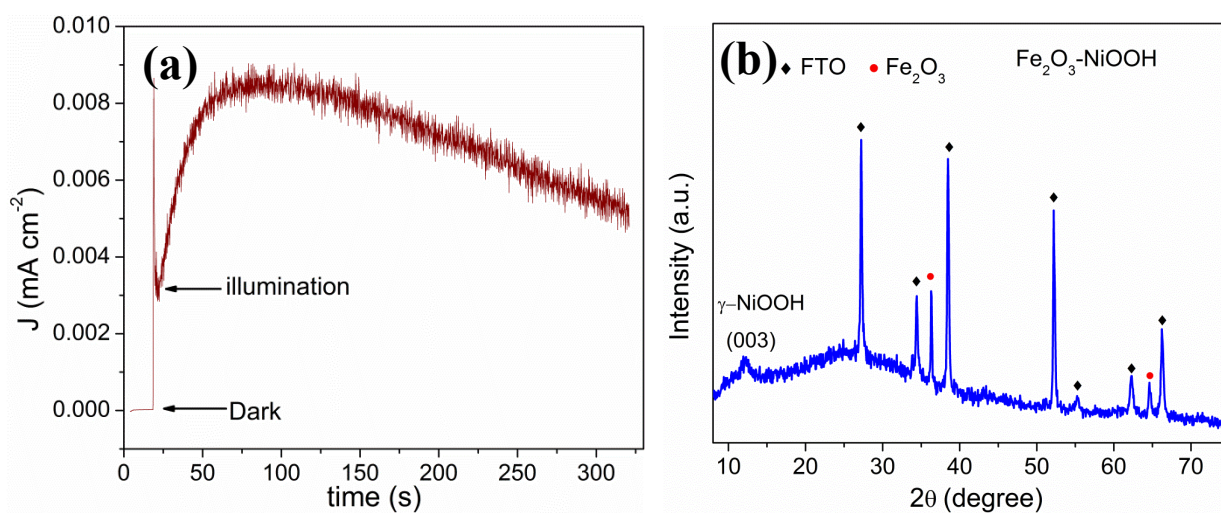


Figure S2. (a) The deposition curve of NiOOH for continuous 5 min. (b) The XRD pattern of the corresponding Fe₂O₃/Fe_{2-x}Sn_xO₃/NiOOH sample.

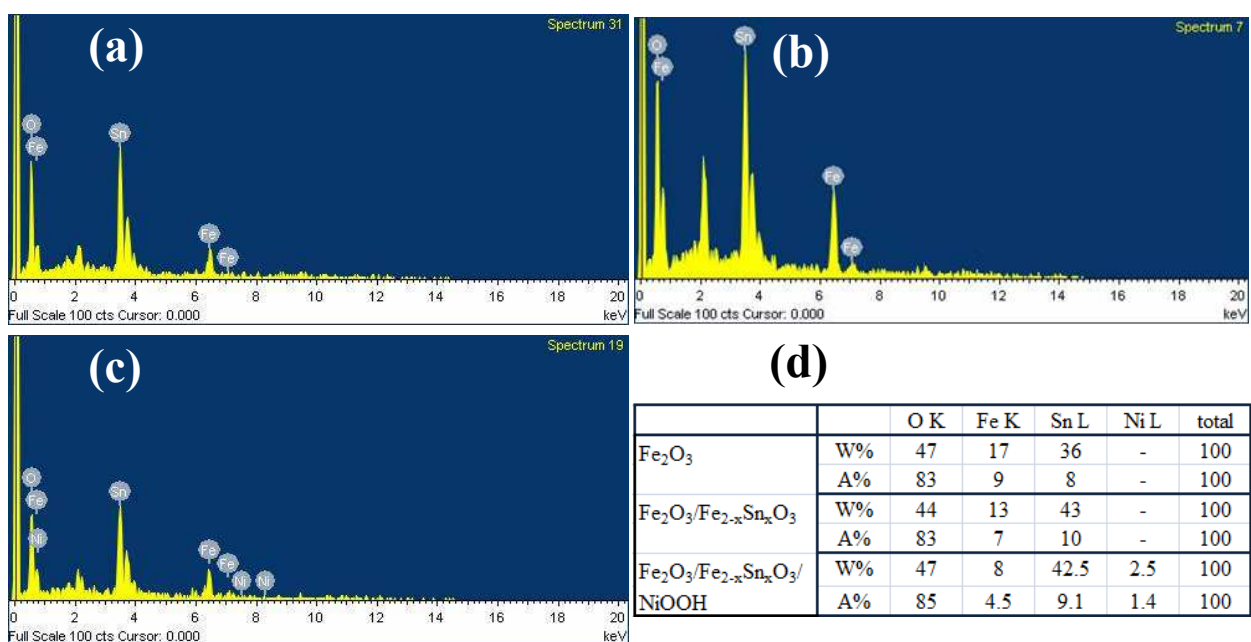


Figure S3. EDS spectra of (a) Fe₂O₃, (b) Fe₂O₃/Fe_{2-x}Sn_xO₃ and (c) Fe₂O₃/Fe_{2-x}Sn_xO₃/ NiOOH. (d) Atomic and weight composition of respective sample.

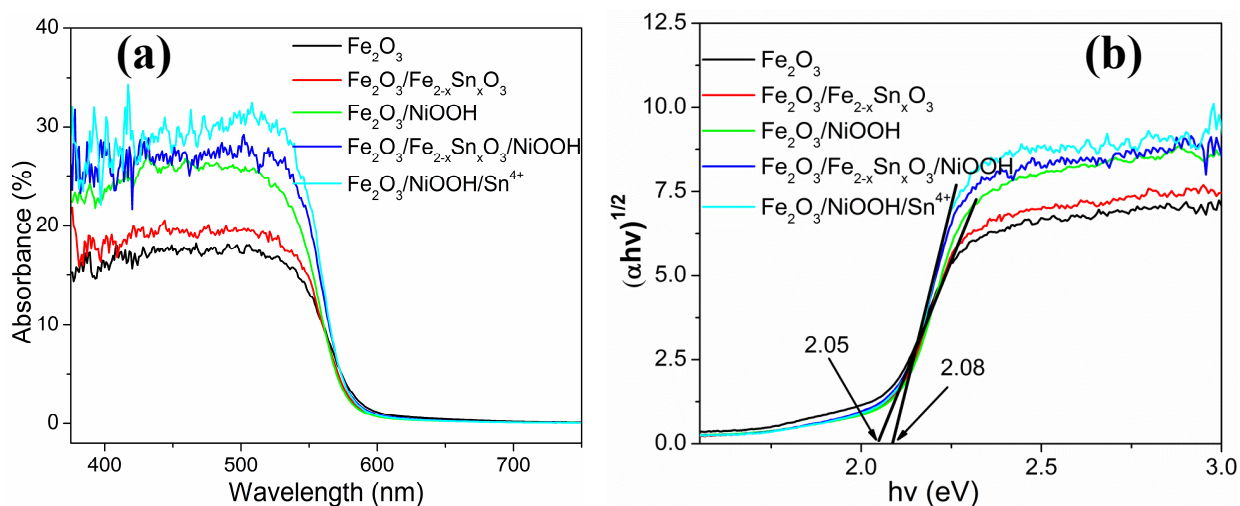


Figure S4. (a) UV-visible absorption spectra of pristine and surface treated Fe₂O₃ samples. (b) Optical band gap of Fe₂O₃ and surface treated Fe₂O₃ samples.

The approximate band gaps of all the samples were determined from Tauc plots (Figure S3). Because hematite is a type of indirect bandgap semiconductor, the curves of $(\alpha h\nu)^{1/2}$ versus $h\nu$ were plotted according to the following equation¹:

$$\alpha h\nu = A(h\nu - E_g)^2$$

where α is the absorption coefficient, A is a proportional constant, h is Planck's constant, ν is the photon frequency, and E_g is the optical band gap energy. Using a linear fit for the straight interval in the region of largest exponential growth; the intercept to the energy axis corresponds to the optical band gap.

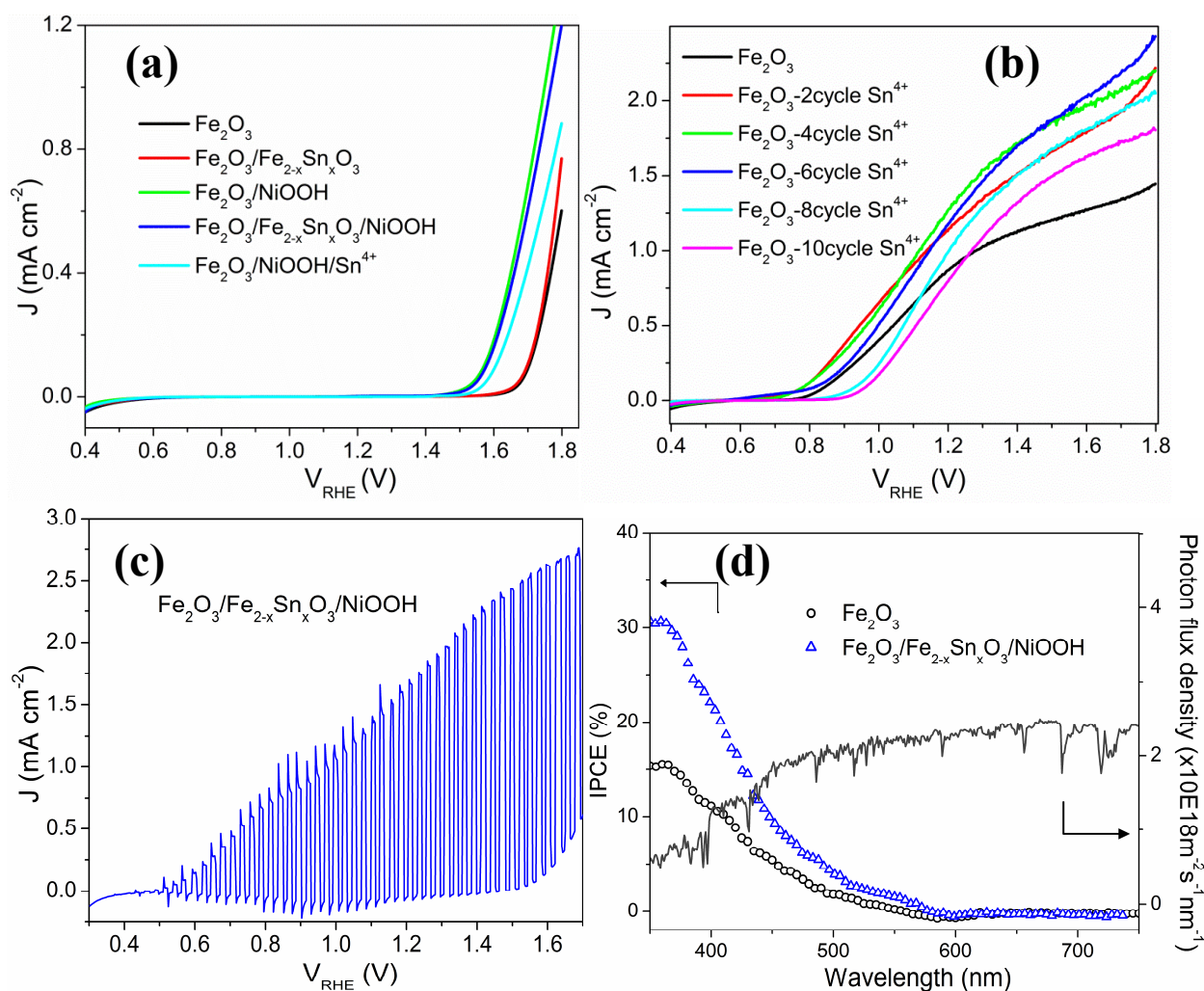


Figure S5. (a) Dark LSV measurements of pristine and surface treated Fe₂O₃ samples. (b) LSV measurements of Sn treated sample with varied number of deposition cycles under illumination. (c) LSV measurement of Fe₂O₃/Fe_{2-x}Sn_xO₃/NiOOH under on/off chopped illumination. (d) IPCE spectra of pristine Fe₂O₃ and Fe₂O₃/Fe_{2-x}Sn_xO₃/NiOOH collected at the incident wavelength range from 350 to 750 nm at a potential of 1.23 V vs RHE (left axis) and AM1.5G spectra converted to photon flux (right axis).

To understand the interplay between the PEC activity and the light absorption properties of samples, we examined their PEC activity as a function of wavelength using photon-to-current conversion efficiency (IPCE) measurements (Fig. S5(d)). The IPCE values of the pristine Fe₂O₃, and Fe₂O₃ sequentially treated with surface Sn doping and NiOOH cocatalyst (*i.e.* Fe₂O₃/Fe_{2-x}Sn_xO₃/NiOOH) are measured at water oxidation potential (1.23 V). The photoresponse of both the samples begins at about 590 nm regardless of the presence of surface passivation layer or catalyst which is consistent with their corresponding UV-visible diffusion absorbance spectra (Fig. S4(a)). This indicates that the anodic photocurrents are mainly originated from the band gap transition of Fe₂O₃, implying that both the NiOOH catalyst and surface Sn treatment have no effect on generating photocurrents. Moreover, the IPCE of Fe₂O₃/Fe_{2-x}Sn_xO₃/NiOOH electrode is 1.7 times higher than that of bare Fe₂O₃ at 400 nm, indicating that the recombination of photoexcited carriers is effectively inhibited through successive surface modification with Sn and loading NiOOH cocatalyst which can accelerate the water oxidation reaction and improve the charge transfer processes.

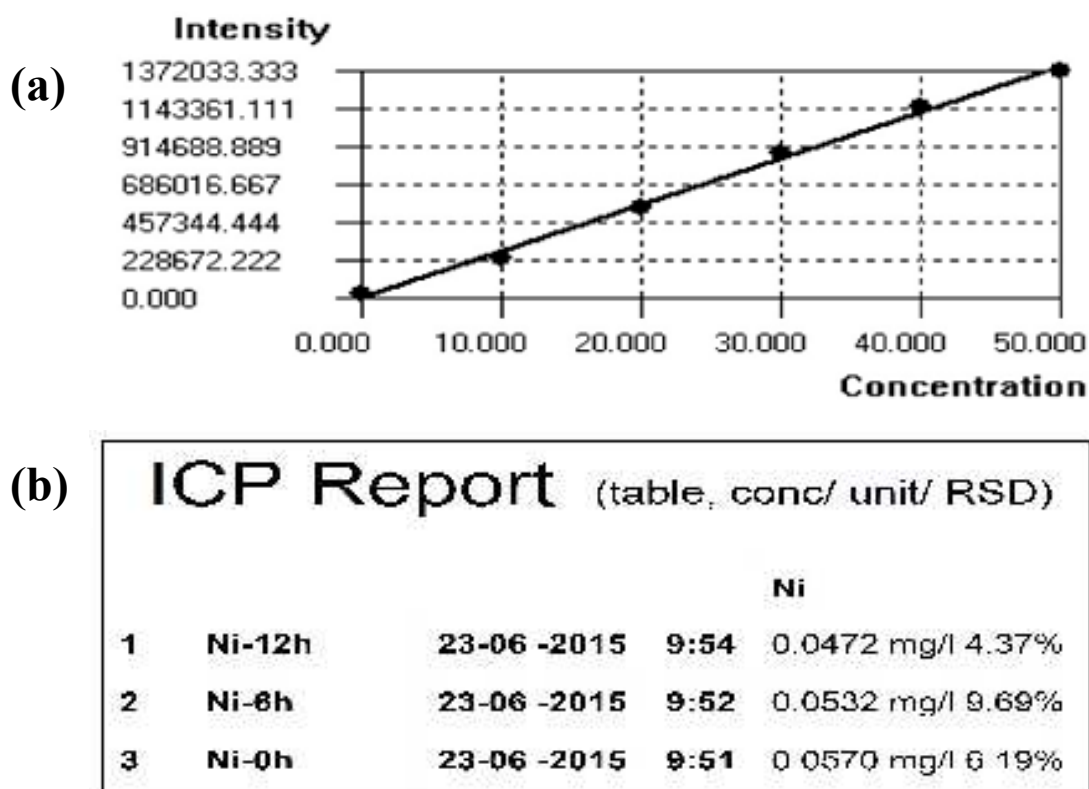


Figure S6. (a) IPC calibration curve containing 0, 10, 20, 30, 40 and 50 ppm Ni solutions. (b) Ni concentrations analysed from electrolyte solutions before and after 6 and 12 h PEC operations.

To get further evidence on the attachment between the NiOOH catalyst and the electrode we analyze the existence of nickel residue in the electrolyte solution after various PEC operation times using

inductively coupled plasma atomic emission spectrometry (ICP-AES). Three different electrolyte samples such as 0, 6 and 12 h PEC operation have been examined. In all cases the amount of Ni found in the electrolyte solution was almost similar *i.e.* nearly zero (Fig. S6(b)). In other words, no nickel dissolution is observed after these long term PEC operation times, suggesting strong attachment between hematite and NiOOH cocatalyst. Considering the high solubility of NiOOH in strongly alkaline solution and the high detection limit of ICP-AES (*i.e.* ppm) we conclude that there is no detachment of the cocatalyst from the electrode.

Mott–Schottky (MS) measurements

In order to elucidate the effects of surface Sn doping and NiOOH cocatalyst on the electronic properties of Fe₂O₃ and hence the enhanced PEC performance, Mott–Schottky (MS) measurements were carried out. Two prominent properties such as donor density and flat band potential (V_{FB}) of the electrodes have been determined by measuring the capacitance of the space charge region formed at the semiconductor/electrolyte interface at a fixed frequency of 1 kHz in dark using the following equation:

$$\frac{1}{C^2} = \frac{2}{\epsilon\epsilon_0 A^2 e N_D} \left(V - V_{fb} - \frac{k_B T}{e} \right)$$

Here, C is the space-charge capacitance of the semiconductor, ϵ is the dielectric constant of hematite (80),² ϵ_0 is the permittivity of vacuum ($8.854 \times 10^{-12} \text{ C V}^{-1} \text{ m}^{-1}$), A is the area of the electrode, e is the electronic charge (1.602×10^{-19}),³ N_D is the number of donors density, V is the applied voltage, V_{fb} is the flat band potential, k_B is Boltzmann's constant, and T is the absolute temperature. So as to fulfill the standard nonlinear relationship between $1/C^2$ and V , some assumption are made in the derivation of the MS equation such as; assuming the much less space-charge region capacitance than the Helmholtz layer capacitance, absence of surface states, frequency-independence of the dielectric constant ϵ , homogeneous spatial distribution of donors/acceptors).^{4,5} Moreover MS is derived from a flat electrode model and may have errors in determining the absolute value of donor density. Here in we made a qualitative comparison of the slopes of the MS plots, given that there is no obvious change of nanowire morphology after surface modification.

The V_{FB} was determined from the intercepts of $1/C^2$ vs. V by subtracting $k_B T/e = 0.025 \text{ V}$ from the intercept (Fig. S7(c)). Table 1(main text) summarizes the V_{FB} and carrier density of the samples. It was found that the pristine Fe₂O₃ photoanode was around 0.39 V which is in line with previously reported values for Fe₂O₃ nanowires. While the surface Sn doped sample (Fe₂O₃/Fe_{2-x}Sn_xO₃) shows nearly the same V_{FB} as that of pristine sample (0.40 V). This shows that the cathodic shift in onset

potential observed in the J-V measurement is as a result of surface passivation layer of the Sn-doped over layer. The V_{FB} of the Fe_2O_3 -NiOOH and $Fe_2O_3/Fe_{2-x}Sn_xO_3/NiOOH$ samples are also not far from the pristine Fe_2O_3 . Considering that these samples exhibit similar V_{FB} , the distinct onset potential observed should not be ascribed to the variation of the V_{FB} in the present work. In case of reverse surface modified sample ($Fe_2O_3/NiOOH/Sn^{4+}$) the V_{FB} shows slight anodic shift. This might be associated with resistance of the Sn^{4+} solution on the transfer of charge across the electrode/electrolyte interface. The charge carrier (donor) density (N_D) is calculated from the slope of the I/C^2 vs. V curve using the following equation.

$$N_D = \left(\frac{2}{\epsilon \epsilon_0 e} \right) [d(1/C^2)/d(V)]^{-1}$$

The results show that the donor density (N_D) of the Sn-doped sample is $3.24 \times 10^{20} \text{ cm}^{-3}$, which is more than one order of magnitude higher than that of the pristine hematite sample ($9.5 \times 10^{19} \text{ cm}^{-3}$), confirming the increment of carriers density of matrix *via* extensive surface Sn doping. This indicates that significant amount of Sn can diffuse to the bulk material during high temperature annealing which acts as an n-type doping and thereby increase the carrier density of the system. The N_D of $Fe_2O_3/NiOOH$ and $Fe_2O_3/Fe_{2-x}Sn_xO_3/NiOOH$ samples are 1.3 and 2.1 times higher than that of the $Fe_2O_3/Fe_{2-x}Sn_xO_3$ sample. This is due to the facilitated charge transfer properties of both samples across the SLJ that decrease interfacial charge recombination. However in case of reversely modified sample ($Fe_2O_3/NiOOH/Sn^{4+}$) the N_D value ($1.05 \times 10^{19} \text{ cm}^{-3}$) is lower than $Fe_2O_3/Fe_{2-x}Sn_xO_3$, $Fe_2O_3/NiOOH$ and $Fe_2O_3/Fe_{2-x}Sn_xO_3/NiOOH$ samples which implies higher surface recombination.

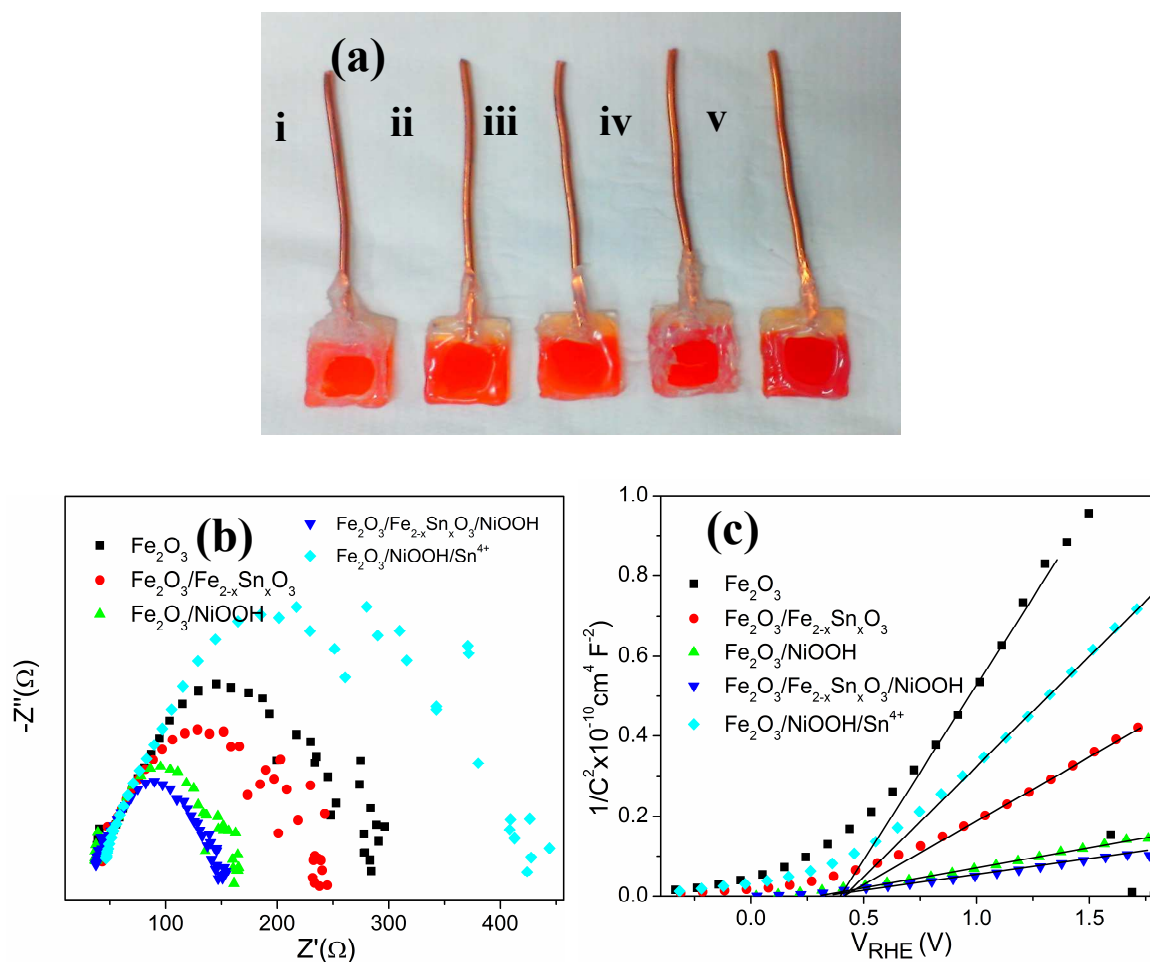


Figure S7. (a) Digital pictures of photoelectrodes covered with epoxy resin (i) Fe_2O_3 (ii) $\text{Fe}_2\text{O}_3/\text{Fe}_{2-x}\text{Sn}_x\text{O}_3$ (iii) $\text{Fe}_2\text{O}_3/\text{NiOOH}$ (iv) $\text{Fe}_2\text{O}_3/\text{Fe}_{2-x}\text{Sn}_x\text{O}_3/\text{NiOOH}$ (v) $\text{Fe}_2\text{O}_3/\text{NiOOH}/\text{Sn}^{4+}$. (b) EIS curves (c) Mott-Schottky plots collected at a frequency of 1 kHz in the dark.

To examine the phase and structural change of the NiOOH cocatalyst up on long term PEC operation we conducted Raman spectra measurements before and after chronoamperometry measurements. In order to examine the top most NiOOH layer of the samples an excitation wavelength of 532 nm with 10% filter was used, which can minimize the Fe_2O_3 signals. Fig. S8(a) and (b) represents the Raman spectra of $\text{Fe}_2\text{O}_3/\text{Fe}_{2-x}\text{Sn}_x\text{O}_3/\text{NiOOH}$ samples after 0, 4, 8, and 12 h PEC operation times. In all the samples two remarkable Raman bands are observed at 473 and 555 cm^{-1} which are attributed to Ni-O vibrations in NiOOH (Fig. S8(a)).^{6,7} Both γ -NiOOH and β -NiOOH exhibit a pair of bands at these wave numbers.⁸ It is reported that in γ -NiOOH the ratio of the intensity of the 473 cm^{-1} band to that of the 555 cm^{-1} band is greater than that for β -NiOOH.⁸ When the PEC operation time increase from

0 to 12 h a considerable increment in intensity is observed at 555 cm^{-1} band. This might be related with the possibility of transformation of γ -NiOOH to β -NiOOH. Louie *et al.* reported that β -NiOOH, for which Ni exists as Ni^{3+} , exhibits a much higher OER activity than γ -NiOOH for which Ni exists as $\text{Ni}^{3.7+}$. Hence, the results here suggest that transformation of γ -NiOOH to β -NiOOH up on long term PEC operation further boosts the OER activity. The disappearance of negative and positive photocurrent spikes observed in the LSV measurement after 12 h chronoamperometry measurement might be associated with this evidence.

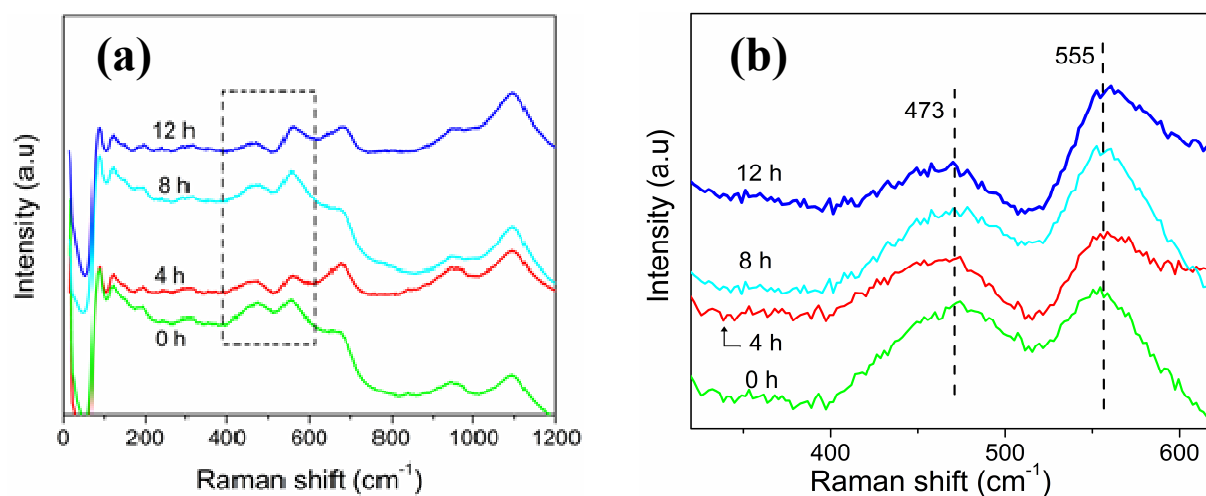


Figure S8. (a) and (b) Raman spectra of $\text{Fe}_2\text{O}_3/\text{Fe}_{2-x}\text{Sn}_x\text{O}_3/\text{NiOOH}$ sample after various operation times.

Water splitting measurements

In order to quantify the Faradaic efficiency, the volume of gas collected per area of electrode and time of gas evolution was recorded every 30 min and the number of moles of gas per area of electrode and time of gas evolution was calculated using the ideal gas law ($n\text{H}_2 = PV/RT$). Then the $n\text{H}_2$ is converted to photocurrent density (using photocurrent density = $2 \times n\text{H}_2 \times F$, where F is the Faraday constant which is $0.096487 \text{ C}/\mu\text{mol}$).

The Faradaic efficiency (FE) was then determined using the expression:

$$\text{FE} = \text{Actual photocurrent density} / \text{Theoretical photocurrent density}^9$$

Based on this calculation, the FE determined was found ranging from 90 to 96% during the whole measurements and the average Faradaic efficiency reached 93%. Thus, more than 90% of the

photogenerated charges were consumed for water splitting and hydrogen/oxygen production in the current system.

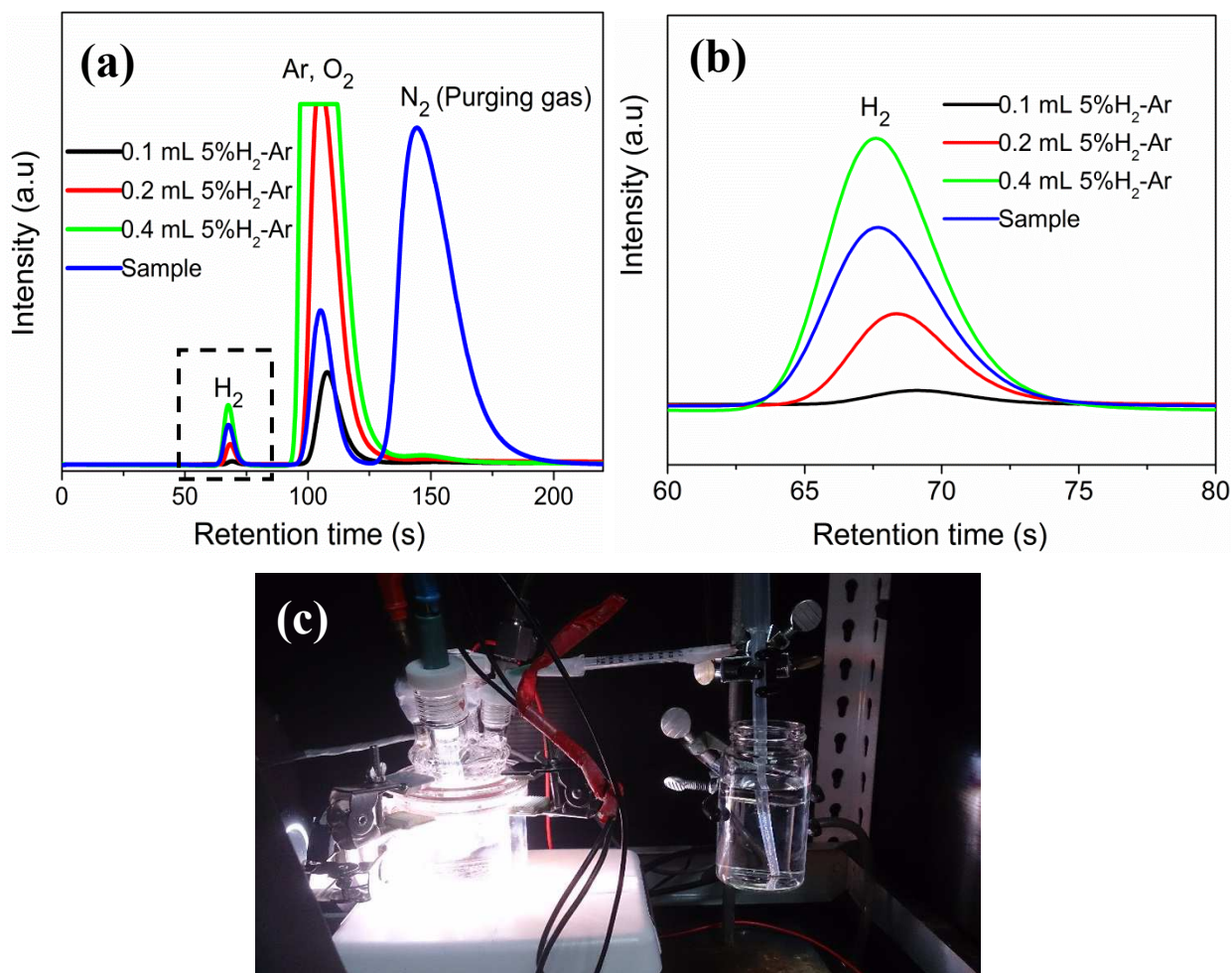


Figure S9. (a) and (b) Standard gas chromatography (GC)-PDHID spectrum of obtained from gas evolution analysis of Fe₂O₃/Fe_{2-x}Sn_xO₃/ NiOOH sample and series of known volumes of 5% H₂-Ar gas samples (0.1, 0.2, 0.4 mL). (c) Photoelectrochemical reactor setup for gas evolution measurement

Stoichiometric oxygen and hydrogen evolution under light driven water splitting are well known to occur with Faradaic efficiencies close to unity in both WO₃ and Fe₂O₃-based systems in an appropriate electrolyte. However, to verify that the measured photocurrent of the photoanode originates from water splitting rather than any other undesired side reactions, a gas evolution experiment was performed at 1.23 V in a gas-tight monolithic PEC cell under continuous illumination and vigorous stirring. The PEC cell contains three electrodes such as Fe₂O₃/Fe_{2-x}Sn_xO₃/NiOOH, Ag/AgCl and Pt plate as working, reference and counter electrodes respectively. A

1 M NaOH electrolyte without any sacrificial reagent and AM 1.5G simulated sunlight was employed. Before the water splitting reaction began, the cell was tightly sealed and purged by Ar for 1 h. Fig. S9(a) and (b) illustrate the gas chromatography (GC) responses of the gas products collected from the water splitting reactor. It was found that hydrogen, oxygen and nitrogen gases are detected at 68, 107 and 145 s retention times. The nitrogen gas signal corresponds to purging gas sample. While hydrogen and oxygen gases are expected from the water splitting reaction.

The water splitting Faradaic efficiency is calculated based on the amount of H₂ produced during the course of the reaction. Because the molar ratio of H₂:O₂ during the entire reaction time was above 2:1 stoichiometric ratio. This is due to the limitation of off-line GC analysis which is highly susceptible for impurity gases from the atmosphere. Moreover, small residual oxygen left in the reactor can cause significant change in the amount of O₂ gas detected. Therefore, we use H₂ gas to determine the amount of O₂ that exactly originates from water splitting based on the expected 2:1 stoichiometric ratio of H₂ and O₂ gases from water splitting. The details of the calculation are given in the supporting information. The amounts of evolved gases as a function of operation time are presented in Table S1. The directly measured photocurrent density, calculated photocurrent converted from the gas measurement and the Faradaic efficiency are depicted in following table. The average Faradaic efficiency was found to be 98%, confirming that the observed photocurrents can be attributed to complete water splitting.

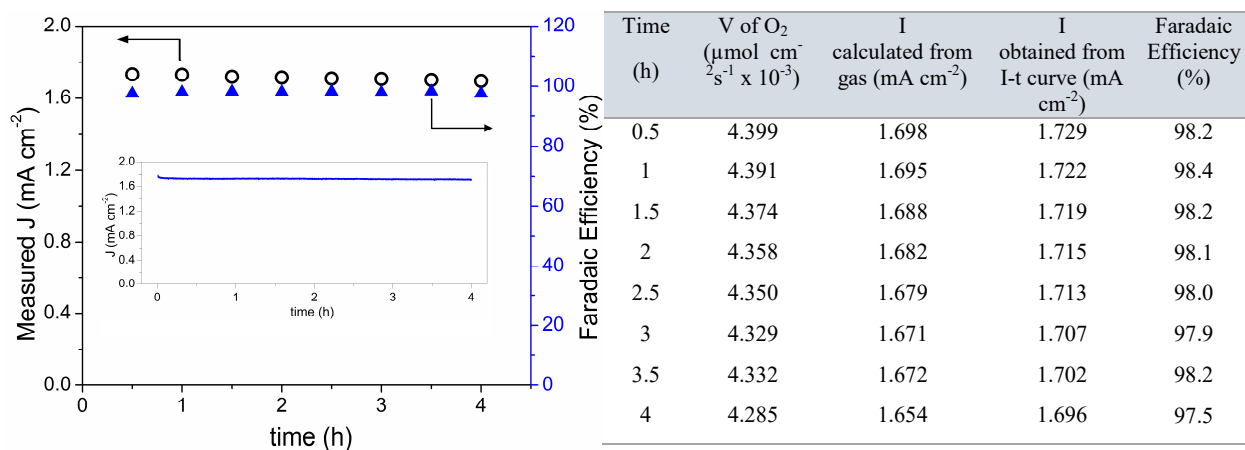


Figure S10. (a) Photocurrent density and Faradaic efficiency measurement for Fe₂O₃/Fe_{2-x}Sn_xO₃/NiOOH photoanode under continuous illumination at 1.23 V vs. RHE in 1 M NaOH electrolyte. Inset: Calculated photocurrent vs. time curve converted from the gas evolution test. (b) Faradaic efficiency calculation for Fe₂O₃/Sn/NiOOH sample from PEC gas evolution measurements.

References

1. P. Wang, D. Wang, J. Lin, X. Li, C. Peng, X. Gao, Q. Huang, J. Wang, H. Xu and C. Fan, *ACS Appl. Mater. Interfaces*, 2012, **4**, 2295-2302.
2. J. Deng, X. Lv, J. Gao, A. Pu, M. Li, X. Sun and J. Zhong, *energy environ. sc.*, 2013, **6**, 1965-1970.
3. K. Gelderman, L. Lee and S. W. Donne, *J. Chem. Educ.*, 2007, **84**, 685-688.
4. R. De Gryse, W. P. Gomes, F. Cardon and J. Vennik, *J. Electrochem. Soc.*, 1975, **122**, 711-712.
5. F. Cardon and W. P. Gomes, *J. Phys. D: Appl. Phys.*, 1978, **11**, L63.
6. Y. L. Lo and B. J. Hwang, *Langmuir*, 1998, **14**, 944-950.
7. M. W. Louie and A. T. Bell, *J. Am. Chem. Soc.*, 2013, **135**, 12329-12337.
8. B. S. Yeo and A. T. Bell, *J. Phys. Chem. C*, 2012, **116**, 8394-8400.
9. Y. Hou, F. Zuo, A. Dagg and P. Feng, *Angew. Chem. Int. Ed.*, 2013, **52**, 1248-1252.